

1 **Synthesis and Antimicrobial Evaluation of Amixicile-Based Inhibitors of the Pyruvate:**
2 **Ferredoxin Oxidoreductases of Anaerobic Bacteria and Epsilon Proteobacteria**

3

4 *Andrew J. Kennedy^a, Alexandra M. Bruce^a, Catherine Gineste^b, T. Eric Ballard^a, Igor N.*
5 *Olekhnovich^b, Timothy L. Macdonald^a and Paul S. Hoffman^{b*}.*

6

7 *Departments of Chemistry^a and Medicine, Division of Infectious Diseases and International*
8 *Health^b, University of Virginia, Charlottesville, Virginia,*

9

10 Running title: Amixicile analogues

11

12 *Corresponding author:

13 Paul S. Hoffman
14 Division of Infectious Diseases and International Health
15 MR4 Bldg, Room 2146
16 409 Lane Road
17 Charlottesville, VA 22908
18 Phone: (434) 924-2893
19 Email: psh2n@virginia.edu

20

21

22 Current addresses:
23 Andrew Kennedy
24 Bates College
25 Department of Chemistry
26 2 Andrews Road
27 Lewiston, Maine 04240
28 Eric Ballard
29 Pharmacokinetics, Dynamics and Metabolism,
30 Pfizer, Inc., Groton, CT 06340, USA

31

32

33

34

35

Abstract

Amixicile is a promising derivative of nitazoxanide (antiparasitic therapeutic) developed to treat systemic infections caused by anaerobic bacteria, anaerobic parasites and by members of the epsilonproteobacteria (*Campylobacter* and *Helicobacter*). Amixicile selectively inhibits pyruvate:ferredoxin oxidoreductase (PFOR) and related enzymes by inhibiting the function of the vitamin B₁ cofactor (thiamin pyrophosphate) by a novel mechanism. Here we interrogate the amixicile scaffold, guided by docking simulations, direct PFOR inhibition assays and by minimal inhibitory concentration (MIC) tests against *Clostridium difficile*, *Campylobacter jejuni* and *Helicobacter pylori*. Docking simulations revealed the nitro group present in nitazoxanide to interact with the protonated N4'-aminopyrimidine of thiamine pyrophosphate (TPP). The *ortho*-propylamine on the benzene ring formed an electrostatic interaction with an aspartic acid moiety (B456) of PFOR that correlated with improved PFOR inhibitory activity and potency by MIC tests. Aryl substitution with electron withdrawing groups and substitutions of the propylamine with other alkyl amines or nitrogen-containing heterocycles both improved PFOR inhibition and in many cases biological activity against *C. difficile*. Docking simulation results correlate well with mechanistic enzymology and NMR studies that show this class of antimicrobials to be specific inhibitors of vitamin B₁ function by proton abstraction which is both novel and likely to limit mutation-based drug resistance.

Introduction

Infectious diseases are a leading cause of death worldwide and antibiotics developed to combat these infections are being lost to the rapid emergence of drug resistance. For most antibiotics that are derivatives of natural products, resistance mechanisms often pre-exist clinical usage and these resistance genes over time tend to accumulate in pathogens via lateral transfer of genetic elements (1, 2, 3). In contrast, synthetic antimicrobials developed against new drug targets where no natural product inhibitor exists are prone to mutation based drug resistance (4, 5). Strategies employing empiric approaches to target identification and high throughput screening of chemical libraries have also failed to deliver new therapeutics to the clinic (1, 2, 6, 7). Several studies have suggested that the number of druggable targets in microbial pathogens is quite small when essentiality, selectivity, catalytic mechanism and chemical space are factored in (7, 8). Thus, identifying new druggable targets is one of the major challenges to the development of next generation antimicrobials. One potential target not found in humans or mitochondria, but common in many human pathogens, is pyruvate: ferredoxin oxidoreductase (PFOR) (9). We discovered that nitazoxanide (NTZ), a synthetic antiparasitic nitrothiazolide therapeutic (Figure 1), inhibits this enzyme by a novel mechanism that does not involve nitroreduction (10, 11).

NTZ completely inhibits the production of acetyl-CoA and CO₂ from pyruvate by out-competing pyruvate for binding to the vitamin B₁ thiamine pyrophosphate (TPP) cofactor of PFOR (K_i value of $\sim 5 \times 10^{-6}$ M, which is roughly two orders of magnitude lower than the K_m value for pyruvate $K_m \sim 3 \times 10^{-4}$ M) (11). The NTZ amide is unusually acidic and is deprotonated at biological pH, producing an anion that is delocalized throughout the thiazole ring. The nitro group of NTZ interacts with and abstracts a proton from the activated N4' aminopyrimidine of TPP, thus inactivating the catalytic cycle (10, 11, 12). The kinetics of protonation can be tracked spectrophotometrically (10). Protonated NTZ is no longer biologically active, but the anion is readily regenerated under physiological conditions (pKa ~ 6.18) (11). Unlike many nitro-

88 containing drugs, the nitro group of NTZ, a weak acid, is not susceptible to nitroreduction or
89 otherwise chemically modified (11, 12, 13). Conceptually, therapeutics that target the function of
90 a vitamin cofactor, itself a small molecule, are unlikely to be amenable to mutation-based drug
91 resistance (11, 14, 18).

92 NTZ is largely retained in the intestine where it is used for the treatment of infections
93 caused by *Cryptosporidium* and *Giardia* (15). Based on several *in vitro* studies (16, 17) and
94 recognizing the potential for a systemic derivative, we chemically interrogated the NTZ scaffold
95 and from ~350 derived analogues, identified an attractive candidate amixicile (Figure 1) that
96 both retained potency and selectivity for PFOR targets and possessed good pharmacokinetic
97 properties (10, 11, 13, 14, 15). In preclinical studies, amixicile showed equivalence with
98 vancomycin and other mainline therapeutics in treatment of *Clostridium difficile* infections (CDI)
99 and similarly with metronidazole in treatment of *Helicobacter pylori* infections in mouse models
100 (14,18). Importantly, amixicile did not accumulate in the mouse cecum or alter the gut
101 microbiome of healthy animals (18). Based on serum binding, it has been suggested that
102 amixicile most likely concentrates in areas of mucosal inflammation via serum leakage where it
103 is active locally against offending susceptible microbes (18). Amixicile differs from NTZ by
104 replacement of the acetoxo group on the benzene ring with propylamine (see Figure 1). We
105 have used a combination of *in silico* PFOR docking simulations and validation via direct PFOR
106 inhibition assays and minimal inhibitory concentration (MIC) determinations to direct lead
107 optimization of the amixicile scaffold. Here we report on several modifications to the amixicile
108 scaffold that improve *in vitro* activity against several susceptible pathogens.

Materials and Methods

Determination of MIC values for *H. pylori* and *C. jejuni* (micro dilution). *H. pylori*

strain 26695 was grown over night at 37 °C under microaerobic conditions in either Brucella broth (BB) or Brain Heart infusion (BHI) medium supplemented with 7.5% serum (4). *C. jejuni* strain H840 was grown in BB medium without supplementation (11). For the microdilution assay, bacterial cultures were diluted to a final OD₆₀₀ of 0.03 for *H. pylori* and 0.01 for *C. jejuni* and 100 µL was dispensed into wells of a 96 well microplate (12, 13). Analogues, either in dimethyl sulfoxide (DMSO) or water, were diluted serially starting at 32 µg/mL in the microtiter plate and the DMSO concentration was always less than 1%. DMSO and NTZ served as controls. Plates were incubated with gentle shaking at 37 °C in a microaerobic incubator (7% O₂ and 10% CO₂). The turbidity in the wells was read visually at 27 h or with a plate reader (Molecular Dynamics). MIC is defined as the concentration of drug that produced no detectable bacterial growth (12).

Determination of MIC Values for *C. difficile* (agar dilution). *C. difficile* strain VPI

10463 was grown anaerobically overnight in chopped meat medium (Anaerobe system) from stock, and it was subcultured to a new chopped meat medium for 5 h at 37 °C (13, 14). It was standardized to an optical density of 0.1 at OD₆₀₀. Analogues were then diluted into the agar media at concentrations ranging from 0.125 - 8 µg/ml. Ten-microliter volumes of the standardized inoculum were delivered to the surface of the agar plates. The number of viable bacteria contained in each inoculum was approximately 7×10^4 and 3.5×10^4 organisms. The plates were incubated for 18 h in an anaerobic chamber and were read visually for growth or no growth. Anaerobic plates containing no compound were used as controls.

138 **PFOR enzyme assay.** *H. pylori* PFOR enzyme was overexpressed and purified from *E.*
139 *coli* as described previously (11, 13). Enzymatic assays were carried out at 25 °C in 1-mL
140 cuvettes in a modified Cary-14 spectrophotometer equipped with an OLIS data acquisition
141 system (On Line Instrument Co., Bogart, Georgia). PFOR (EC 1.2.7.1) was assayed under
142 anaerobic conditions with 100 mM potassium phosphate (pH 7.4), 10 mM sodium pyruvate, 5
143 mM benzyl viologen (BV; $\epsilon=9.2 \text{ mM}^{-1} \text{ cm}^{-1}$ at 546 nm), 0.18 mM CoA, and 1 mM MgCl_2 . The
144 reaction was started by addition of enzyme, in the presence or absence of inhibitor (NTZ or its
145 derivative in concentration of 40 μM) and the reduction of redox-active BV dye was monitored at
146 546 nm. Inhibition of PFOR was expressed in percent with NTZ set at 50%.

147
148 **Docking simulations.** Docking simulations (MOE; molecular operating environment
149 20010.0 release by Chemical Computing Group) with the 1.87 Å crystal structure of PFOR from
150 *Desulfovibrio africanus* (PDB 1B0P) (19, 20, 21) were performed to rationalize the proposed
151 mechanism of action of NTZ and AMX (11, 12). Anionic NTZ, TZ, and amoxicillin were docked
152 into the PFOR crystal structure using the triangle match algorithm, biasing the nitro group to
153 remain within 5 Å of TPP, and potential modes of binding were assessed by estimating the free
154 energy of binding using the Merck molecular force field and the London dG scoring function,
155 which estimates enthalpic interactions within the binding pocket, the energy of desolvation, and
156 the cost of rigidifying freely rotatable bonds. The docking studies indicated that the 5-nitro group
157 of 2AT directly interacts with TPP and the binding pocket's residues Arg B114 and Thr B31.
158 Additionally, the amide carbonyl accepted a hydrogen bond from Asn B996. The *in silico* studies
159 suggest that improved binding of amoxicillin might result from electrostatic interactions of the
160 amine tail with the acidic side chain of Asp B456 that mediates acetylation of coenzyme A in the
161 pocket, taking advantage of unexplored chemical space and leading to better selectivity. This
162 knowledge, combined with the previous studies of benzene ring substitution, allow for further
163 derivatives of AMX to be explored.

164

165 General chemistry methods, chemical synthesis and analysis of analogues.

166 Details on chemistry, synthesis and purity of compounds can be found in the supplemental
167 materials (S1).

168

169

170

Results

171

172 Our strategy for further development of the amixicile scaffold is based on previous
173 unpublished work associated with docking simulations with nitazoxanide (NTZ) and its active
174 metabolite tizoxanide (TZ, the phenol) with the crystal structure of PFOR from *Desulfovibrio*
175 *africanus* (20, 21). Previous mechanistic and NMR studies indicated that NTZ interferes with the
176 PFOR enzymatic reaction as a competitive inhibitor of pyruvate binding to TPP (11). Therefore,
177 the PFOR crystal structure in which pyruvate is bound (but not reacting) was chosen for the
178 development of the homology model. Since the carboxylate moiety of pyruvate forms a
179 hydrogen bond to the thiamine pyrophosphate (TPP) cofactor of PFOR (19), the electron-rich,
180 isosteric nitro group of NTZ was placed in the active site in a similar conformation. The head
181 group, amide linker and benzene ring of amixicile were then built into the PFOR pocket and a
182 library of conformers was assembled and screened. Those conformations that had the lowest
183 calculated binding affinity in a rigid enzyme model were minimized and re-scored, this time
184 allowing both the ligand and amino acid side-chains in the active site to resolve torsional strain
185 and ligand collisions, while holding the protein backbone and non-active site residues rigid. The
186 best scoring orientation became the template for second-generation NTZ analogues. With this
187 as a guide, various tail groups and benzene linker substitution patterns were built, screened and
188 scored to predict their efficacy *in vitro*. Figure 2A depicts the interaction of TPP with pyruvate
189 showing the carbonyl oxygen interacting with the aminopyrimidine. The carbanion of the thiazole
then attracts the positively charged carbonyl of pyruvate to form the lactyl-TPP intermediate. As

190 seen in Figure 2B, the anion of the tizoxanide is predicted to interact with TPP via the N4'-
191 aminopyrimidine. In this model, TPP forms a V shape that enables the thiazole carbanion to be
192 relatively stable and the N4' to be essentially protonated in the activated state (19). Amixicile
193 appears to bind and function mechanistically similar to NTZ, but the steric bulk and cation of the
194 propyl amine better fills the substrate pocket and forms a weak ionic interaction with Asp B456.
195 As seen in Figure 2D (docking with amixicile), the chemical space of the catalytic cavity is rather
196 large (30 Å), suggesting room for further chemical development. Alignments of other PFOR
197 amino acid sequences (BLASTP) in key regions show that several active site amino acids, such
198 as ThrB31, GluB64 and ArgB114, are highly conserved. Docking simulations with amixicile
199 show probable interactions, not only with the N4' of the aminopyrimidine, but also hydrogen
200 bonds with ArgB114 and ThrB31 with the nitro group oxygens, AsnB996 with the keto group of
201 the amide bond and AspB456 with the protonated amine of the propylamine moiety (see Figure
202 3A). Figure 3B shows the relationship of TPP, amixicile and the three 4Fe:4S redox centers
203 which show considerable chemical space in which to drive further development. Moreover, the
204 benzene ring fits into a trough in the enzyme (Figure 3B) that might be amenable to SAR
205 development to improve binding efficiency.

206 A conclusive SAR was required to set rational structural limits and propose compounds
207 that would optimize binding interactions at PFOR. Previous studies by our group and those of
208 others have focused on the 2ANT moiety and benzene ring (12, 13, 14). The addition of a
209 propylamine tail to the NTZ scaffold introduced a new region for optimization that could lead to
210 more potent inhibitors in whole cells. Some thought was also directed to the possibility that the
211 reaction of analogues with TPP might be augmented by additional substituents on the ring that
212 might kinetically improve the inhibitory action. To design such inhibitors, the amixicile scaffold
213 was broken down into three parts for structural analysis (Figure 4). Studies then focused on the
214 linker and tail regions for further development.

215

216 **Tail region optimization.** To begin optimizing the structure of amixicile, the length of the
217 tail region was analyzed. The tail in the *ortho*- position was systematically shortened,
218 lengthened and rigidified to determine the optimal length and presentation allowed in the PFOR
219 pocket. Compounds were prepared by first coupling the commercially available methyl
220 benzoate or aldehyde to the desired tail region coupling partner under Suzuki conditions (Figure
221 5) (22). Once the tail group was added, the resulting ester or aldehyde was hydrolyzed or
222 oxidized to the respective carboxylic acid via saponification or Pinnick oxidation (13, 23).
223 Finally, the 2-amino-5-nitrothiazole (2ANT) head group was appended using EDC coupling
224 methods previously described and the amine was deprotected to form the hydrochloric acid salt
225 (12, 13). This provided a logical series of derivatives to assess the spatial tolerance of the
226 PFOR pocket. The computational study indicated a potential electrostatic interaction between
227 the amine tail and Asp B456 that could be amplified by adjusting the length and structural fluidity
228 of the tail group. The small library was subjected to direct PFOR inhibition assays to assess
229 preliminary activity at the enzyme (Figure 6) (11,12).

230 Modifying the amine tail from zero to four carbons allowed for the area of the PFOR
231 pocket facing away from the active site to be analyzed. Preliminary PFOR inhibition assays
232 revealed that activity drops when the spacer is less than three carbons. When the spacer was
233 four carbons, PFOR inhibition increased but this did not translate into lower, more potent, MIC
234 values against target pathogens. Due to the high cost of the coupling partner required for 4.3
235 and 4.4, further optimization studies were performed using the propylamine tail of amixicile for
236 preliminary analysis.

237
238 **Optimization of the benzene ring of amixicile.** A new series of amixicile derivatives
239 were synthesized using the propylamine tail in the *ortho*-position (Figure 7). Previous SAR
240 studies, while largely inconclusive, provided clues to substituents that could further increase
241 inhibitory activity of the PFOR enzyme and in whole cells (20). Electron-donating and

242 withdrawing groups (EDG and EWG, respectively) were added to the benzene ring linker region
243 of amixicile to establish a correlation between the spatial and electronic properties of the ring in
244 the pocket and activity. The inhibitory activities of these analogues at 40 μ M are listed in Figure
245 7. All of these compounds showed greater inhibitory activity than did NTZ and amixicile.
246 Importantly, these compounds retained selectivity for PFOR containing bacteria and showed no
247 inhibitory activity against non-PFOR-containing bacteria like *E. coli* and *S. aureus* (>32 μ g/mL,
248 data not presented). Similarly, CC₅₀ determinations with HeLa cells revealed none of these
249 derivatives was toxic at concentrations below 100 μ g/ml (data not presented). In accordance
250 with previous trends, R² and R³-substituted compounds 4.12 – 4.17 were comparable to
251 amixicile in potency against *C. difficile in vitro* by MIC tests, with R³ CH₃ 4.12 showing the
252 greatest improvement in activity (0.06 μ g/ml versus amixicile 0.125 μ g/ml). Despite this
253 enhanced activity, the compounds were not as active as NTZ against *C. difficile* (Figure 7).
254 Interestingly, meta-substituted (R²) compounds 4.10 and 4.11, had the second lowest MIC value
255 of 0.0625 μ g/ml against *C. difficile* and much greater percent inhibition of PFOR inhibition of
256 97% and 93% respectively. MIC results are often a function of drug uptake or efflux, factors that
257 do not influence IC₅₀ tests. These data show a marked improvement compared to previous
258 studies of compounds without the propylamine tail (12, 13). Of all the substitution patterns,
259 electron withdrawing groups in the R² (meta-) position have shown the greatest increase in
260 activity and potency.

261 The meta-substitution pattern of 4.8, 4.10 and 4.11 corresponds well with *in silico*
262 docking studies of amixicile, which shows a cavity that can accommodate substituents in the R²
263 position. This pocket, while small, was calculated to be large enough to accept small
264 substituents, such as fluorine, chlorine, methyl, and trifluoromethyl (CF₃). Even though these
265 groups have different electron withdrawing effects, all four substituents improved potency,
266 suggesting that steric effects drive the observed improvements in performance.

267

268 Despite the enhanced potency, there continue to be inconsistencies between *in vitro*
269 enzyme and *in vivo* whole cell data. The percent PFOR inhibition has nearly doubled from NTZ,
270 yet the MIC values for respective compounds remain only two or three fold those of NTZ (Figure
271 7). This may not be detrimental to the overall goal, however, as amixicile still outperforms NTZ
272 in a CDI mouse model even with this discrepancy (14). While hydrophobicity can affect drug
273 uptake or efflux, evaluation of cLogP values for the analogues did not correlate with biological
274 activity.

275

276

277

278

279

Discussion

280

281 We have used a combination of docking simulations, enzymology and MIC testing of
282 selected susceptible bacteria to direct development of second generation PFOR inhibitors
283 based on the amixicile scaffold. Initial mechanistic studies indicated that these 2ANT
284 derivatives exhibit extensive electron delocalization of the negative charge generated by amide
285 deprotonation and our docking simulations indicated that the resonance contributor with an
286 anionic 5-nitro group is the most likely electronic resonance form to interact with and abstract a
287 proton from the N4' amino pyrimidine group of TPP. Docking simulations also supported
288 previous conclusions that the nitro group is essential to the biological activity and that this
289 activity can be influenced by coupled substituents (12, 13, 14). Docking simulations also
290 confirmed that the chemical space within PFOR was large and therefore can accommodate
291 large bulky substituents (12, 13). We determined that the propylamine tail chain length was
292 optimized and is predicted to interact with Asp B456. Since protonated amixicile and analogues
are rapidly deprotonated by water (pKa 6.2), these secondary interactions within this chemical

293 space might maintain drug proximity to TPP and thereby improve efficiency against the
294 reactivated enzyme. In this regard, we have shown that a large variety of heterocycles similarly
295 coupled to 2ANT exhibit increased inhibitory action in direct PFOR assays and in potency
296 against a wide range of PFOR containing bacteria and anaerobic parasites (11).

297 The second premise driving SAR was that on the phenyl ring strong electron
298 withdrawing groups would enhance biological activity at PFOR and electron-donating ones
299 would not. However, our studies found that halide substitutions at position (R^2) were only
300 incrementally improved over methyl and trifluoromethyl groups as indicated by PFOR inhibitory
301 testing and by MIC for the selected susceptible pathogens. We also found that rigidifying the
302 propylamine tail of amixicile into the cyclized piperidine (Figure 6) also improved potency
303 against PFOR. However, these compounds were less soluble in water which might affect
304 bioavailability for systemic use. The structures are clearly amenable to further substitution by
305 halides, propylamine and perhaps other heterocycles in a directed SAR strategy. Similarly and
306 based on previous studies, the 2ANT head group is amenable to further development as
307 dinitrothiophene derivatives show potency against PFOR by enzyme assay and by direct MIC
308 tests (12,13). These derivatives have not been analyzed in docking simulations that might infer
309 additional interactions within the catalytic pocket.

310 We noted variation in potency (MIC) of compounds against PFOR expressing bacteria,
311 with *C. jejuni* exhibiting higher MICs when compared with *C. difficile* and *H. pylori*. Pyruvate
312 metabolism is far more diverse in *C. jejuni* suggesting that PFOR might be a less robust target
313 in this species (11, 14). Overall, our SAR strategy led to more potent analogues based on *in*
314 *vitro* studies. While docking simulations directed synthesis we found that potency for inhibition of
315 PFOR did not necessarily correlate with MIC. The greater potency of some analogues for Gram
316 positive *C. difficile* versus *H. pylori* or *C. jejuni* is likely due to penetrability through two
317 membranes in the Gram negatives. The length of the alkyl tail also affected aqueous solubility
318 as cLogP values increased with carbon length, again with the propylamine being optimal for

319 both MIC and cLogP (amixicile). Whether these more potent leads also retain the excellent
320 DMPK, cytotoxicity metrics and efficacy of amixicile will require further study. Preliminary testing
321 of selected analogues in a mouse CDI model showed that analogue 4.11 (2-trifluoromethane
322 derivative) was well tolerated in a lethal challenge mouse CDI model (20 mg/kg/day for 5 days)
323 with minimal weight loss and no diarrhea. However a related analogue 4.10 (2-chloro) was not
324 well tolerated and infected animals exhibited greater weight loss and diarrhea. These
325 preliminary studies indicate that animal studies will be required to delineate toxicity versus
326 efficacy. Since the vast majority of new antimicrobials developed for the CDI market are poorly
327 absorbed, we cannot rule out the possibility that poorly absorbed analogues might be good
328 candidates for this indication.

329 In this study, the homodimeric PFOR from *Desulfovibrio africanus* was used in modeling
330 studies. PFORs can also be comprised of subunits ranging from 3 to 4 that form the
331 homodimeric oligomer that reconstitutes the catalytic site and in which the key amino acids are
332 conserved (9). For example, the *H. pylori* PFOR is the product of a 4 gene operon as is the
333 oxoacid: ferredoxin oxidoreductase (10, 11, 24). In *C. jejuni* and *C. difficile*, PFOR is expressed
334 from a single gene and forms a homodimer. Remarkably, the core structure, positioning of TPP
335 and the catalytic mechanism are functionally conserved. A QSAR study of the PFOR from
336 *Entamoeba histolytica* in docking simulations with NTZ and benzylthiazoles concluded that
337 these compounds could not replace TPP (25), confirming earlier studies (26). However, studies
338 with the *E. histolytica* enzyme (homodimer), while confirming our previously reported
339 mechanism, did not provide specific interactions of NTZ with the vitamin cofactor of PFOR.
340 Since the study did not model pyruvate, it is possible that the enzyme was not in a catalytically
341 activated state as set up in our modeling studies. Since considerable conformational change
342 occurs during activation and catalysis (19), we believe our docking simulations are a good fit to
343 the previously reported experimental data (19). Moreover, we confirmed experimentally with

344 purified PFOR from *E. histolytica* that NTZ was both a substrate of and an inhibitor of the
345 enzyme which supports the proton abstraction mechanism (11).

346 One of the greatest challenges to the development of new antimicrobials is finding new
347 drug targets, especially ones with mechanisms that might escape or delay the inevitable
348 development of antimicrobial resistance. Our modeling simulations and SAR strategy show that
349 vitamin B₁ is the target of NTZ, amoxicillin and analogues. Consistent with this notion, we and
350 others have not been successful using laboratory conditions to generate mutants resistant to
351 NTZ or amoxicillin (10, 11, 14, 18). Similarly, there are no reports of resistance to NTZ from its use
352 clinically. While we anticipate that the analogues will also escape mutation based drug
353 resistance, this has not been confirmed experimentally. Our studies do not rule out second-site
354 mutations or changes in gene expression (efflux genes) that might contribute to increased
355 resistance to these analogues. In this regard, we do know that metronidazole-resistant strains of
356 *H. pylori* show some cross-resistance to NTZ, amoxicillin and analogues (18). The noted cross-
357 resistance appears to result from incremental increases in PFOR gene expression and to
358 compensatory metabolic activities that increase tolerance, rather than to mutations within PFOR
359 or vitamin that can be transferred genetically to susceptible strains (10). This noted incremental
360 tolerance can be overcome by drug concentrations above MIC that are readily achievable
361 clinically (18).

362 In summary, we have used docking simulations with amoxicillin together with direct
363 enzyme assay and MIC testing to identify analogues of amoxicillin with increased inhibitory action
364 against PFOR containing bacterial pathogens. Our studies further show that the PFOR target is
365 amenable to further space filling chemical development, as long as the anionic nitro group of the
366 thiazole is maintained. This interaction with the protonated N4' aminopyrimidine is required for
367 inactivation of the PFOR catalytic cycle. To our knowledge, this is the first example of an
368 antimicrobial therapeutic that specifically targets the mechanism of action of a vitamin cofactor

369 and not the enzyme directly. Perhaps similar drug discovery strategies can be used to probe
370 other unique microbial enzymes which rely on a vitamin cofactor for biological activity.

371

372

373

374

Acknowledgements

375 We thank Jennifer L. Tomlinson and Xia Wang for technical assistance. This project was funded
376 by National Institute of Allergy and Infectious Diseases, National Institutes of Health,
377 Department of Health and Human Services grants U01 AI075520 and R21AI111604 to PSH.

378

379

380

References

- 381 1. **Silver LL**. 2011. Challenges of antibacterial discovery. Clin Microbiol Rev. **24**:71-109.
- 382 2. **Devasahayam G, Scheld MW, Hoffman PS**. 2009. Newer antimicrobials for a new century.
383 Expert Opinion on Investigational Drugs, **19**:215-34.
- 384 3. **Boucher HW, Talbot GH, Bradley JS, Edwards JE, Gilbert D, Rice LB, Scheld M,**
385 **Spellberg B, Bartlett J**. 2009. Bad bugs, no drugs: no ESKAPE! An update from the
386 Infectious Diseases Society of America. Clin Infect Dis **48**:1-12.
- 387 4. **Sisson G, Jeong JY, Goodwin A, Bryden L, Rossler N, Lim-Morrison S, Raudonikiene**
388 **A, Berg DE, Hoffman PS**. 2000. Metronidazole activation is mutagenic and causes DNA
389 fragmentation in *Helicobacter pylori* and in *Escherichia coli* containing a cloned *H. pylori*
390 RdxA(+) (Nitroreductase) gene. J Bacteriol. **182**:5091-5096.
- 391 5. **O'Dwyer K, Spivak AT, Ingraham K, Min S, Holmes DJ, Jakielaszek C, Rittenhouse S,**
392 **Kwan AL, Livi GP, Sathe G, Thomas E, Van Horn S, Miller LA, Twynholm M, Tomayko**
393 **J, Dalessandro M, Caltabiano M, Scangarella-Oman NE, Brown JR**. 2015. Bacterial

- 394 resistance to leucyl-tRNA synthetase inhibitor GSK2251052 develops during treatment of
395 complicated urinary tract infections. *Antimicrob Agents Chemother.* **59**:289-298.
- 396 6. **Payne DJ, Gwynn MN, Holmes DJ, Pompliano DL.** 2007. Drugs for bad bugs: confronting
397 the challenges of antibacterial discovery. *Nature Rev. Drug Discovery.* **6**:29-40.
- 398 7. **Durrant JD, Amaro RE.** 2015. Machine-learning techniques applied to antibacterial drug
399 discovery. *Chem Biol Drug Des.* **85**:14-21.
- 400 8. **Chalker AF, Minehart MW, Hughes NJ, Koretke KK, Lonetto MA, Brinkman KK, Warren**
401 **PV, Lupas A, Stanhope MJ, Brown JR, Hoffman PS.** 2001. Systematic identification of
402 selective essential genes in *Helicobacter pylori* by genome prioritization and allelic
403 replacement mutagenesis. *J. Bacteriol.* **183**:1259-1268.
- 404 9. **Horner DS, Hirt RP, Embley TM.** A single eubacterial origin of eukaryotic
405 pyruvate:ferredoxin oxidoreductase genes: Implications for the evolution of anaerobic
406 eukaryotes. *Mol. Biol. Evol.* **16**:1280-1291.
- 407 10. **Sisson G, Goodwin A, Raudonikiene A, Birks NJ, Han H, Mukhopadhyay A, Berg DE,**
408 **Hoffman PS.** 2002. Enzymes Associated with the Reductive Activation and Action of
409 Nitazoxanide, Nitrofurans and Metronidazole in *Helicobacter pylori*. *Antimicrob. Agents and*
410 *Chemother.* **46**: 2116-2123.
- 411 11. **Hoffman PS, Sisson G, Croxen MA, Welch K, Harman WD, Cremades N, Morash MG.**
412 2007. Antiparasitic drug nitazoxanide inhibits the pyruvate oxidoreductases of *Helicobacter*
413 *pylori* and selected anaerobic bacteria and parasites, and *Campylobacter jejuni*. *Antimicrob*
414 *Agents Chemother.* **51**:868-876.
- 415 12. **Ballard TE, Wang X, Olekhnovich I, Koerner T, Seymour C, Hoffman PS, Macdonald**
416 **TL.** 2010. Biological activity of modified and exchanged 2-amino-5-nitrothiazole amide
417 analogues of nitazoxanide. *Bioorg Med Chem Lett.* **20**:3537-3539.
- 418 13. **Ballard TE, Wang X, Olekhnovich I, Koerner T, Seymour C, Salamoun J, Warthan M,**
419 **Hoffman PS, Macdonald TL.** 2011. Synthesis and antimicrobial evaluation of nitazoxanide-

- 420 based analogues: identification of selective and broad spectrum activity. ChemMedChem.
421 **6**:362-377.
- 422 14. **Warren CA, van Opstal E, E. Ballard TE, Kennedy A, Wang X, Riggins M, Olekhnovich**
423 **I, Warthan M, Kolling GL, Guerrant RL, Macdonald TL, Hoffman PS.** 2012. Amixicile: A
424 novel inhibitor of pyruvate: ferredoxin oxidoreductase shows efficacy against *Clostridium*
425 *difficile* in a mouse infection model Antimicrob. Agents Chemother. **56**:1403-1411.
- 426 15. **Gilles HM, Hoffman PS.** 2002. Treatment of intestinal parasitic infections: A review of
427 nitazoxanide. Trends in Parasitol. **18**:95-97.
- 428 16. **Dubreuil L, Houcke X, Mouton Y, Rossignol JF.** 1996. *In vitro* evaluation of the activities
429 of nitazoxanide and tizoxanide against anaerobes and aerobic organisms. Antimicrob
430 Agents and Chemother. **40**:2266-2270.
- 431 17. **Pankuch GA, Appelbaum PC.** 2006. Activities of tizoxanide and nitazoxanide compared to
432 those of five other thiazolides and three other agents against anaerobic species. Antimicrob.
433 Agents Chemother. **50**:1112-1117.
- 434 18. **Hoffman PS, Bruce AM, Olekhnovich I, Warren CA, Burgess SL, Hontecillas Viladomiu**
435 **RM, Bassaganya-Riera J, Guerrant RL, Macdonald TL.** 2014. Preclinical studies of
436 amixicile, a systemic therapeutic developed for treatment of *Clostridium difficile* infections
437 that also shows efficacy against *Helicobacter pylori*. Antimicrob Agents and Chemother.
438 **58**:4703-4712.
- 439 19. **Chabriere E, Vernede X, Guigliarelli B, Charon M-H, Hatchikian EC, Fontecilla-Camps**
440 **JC.** 2001. Crystal structure of the free radical intermediate of pyruvate:ferredoxin
441 oxidoreductase. Science. **294**:2559-2563.
- 442 20. **Alvarado O, Jana G, Delgado EJ.** 2012. Computer-assisted study on the reaction between
443 pyruvate and the ylide in the pathway leading to lactyl-ThDP. J. Comput. Aided Mol. Des.
444 **26**:977-982.

- 445 21. **Charon M, Volveda A, Chabriere E, Pieulle L, Fontecilla-Camps JC.** 1999. Structure and
446 electron transfer mechanism of pyruvate: ferredoxin oxidoreductase. *Curr Opin. Struct Biol.*
447 **9**:663-669.
- 448 22. **Kamatani A, Overman LE.** 1999. A Suzuki coupling method for directly introducing a
449 protected β -aminoethyl group into arenes and alkenes. convenient synthesis of phenethyl
450 and homoallylic amines. *J. Org. Chem.* **64**: 8743-8744.
- 451 23. **Li Y, Combs A, Yue E, Li H.** 2014. Substituted fused aryl and heteroaryl derivatives as
452 PI3K inhibitors. US Patent No. 8,680,108.
- 453 24. **Hughes NJ, Chalk PA, Clayton CL, Kelly DJ.** 1995. Identification of carboxylation
454 enzymes and characterization of a novel four-subunit pyruvate:flavodoxin oxidoreductase
455 from *Helicobacter pylori*. *J Bacteriol.* **177**:3953-9.
- 456 25. **Scior T, Lozano-Aponte J, Ajmani S, Hernández-Montero E, Chávez-Silva F,**
457 **Hernández-Núñez E, Moo-Puc R, Fraguera-Collar A, Navarrete-Vázquez G.** 2015.
458 Antiprotozoal nitazoxanide derivatives: Synthesis, bioassays and QSAR study combined
459 with docking for mechanistic insight. *Curr Comput Aided Drug Des.* **11**:21-31.
- 460 26. **St Maurice M, Cremades N, Croxen MA, Sisson G, Sancho J, Hoffman PS.** 2007.
461 Flavodoxin:quinone reductase (FqrB): a redox partner of pyruvate:ferredoxin oxidoreductase
462 that reversibly couples pyruvate oxidation to NADPH production in *Helicobacter pylori* and
463 *Campylobacter jejuni*. *J Bacteriol.* **189**:4764-4773.

464
465
466
467
468
469
470

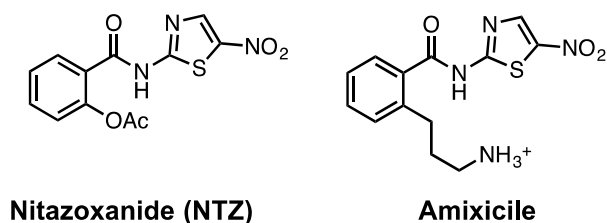


Figure 1. Structures of nitazoxanide and amoxicillin. Tizoxanide is the phenol of NTZ.

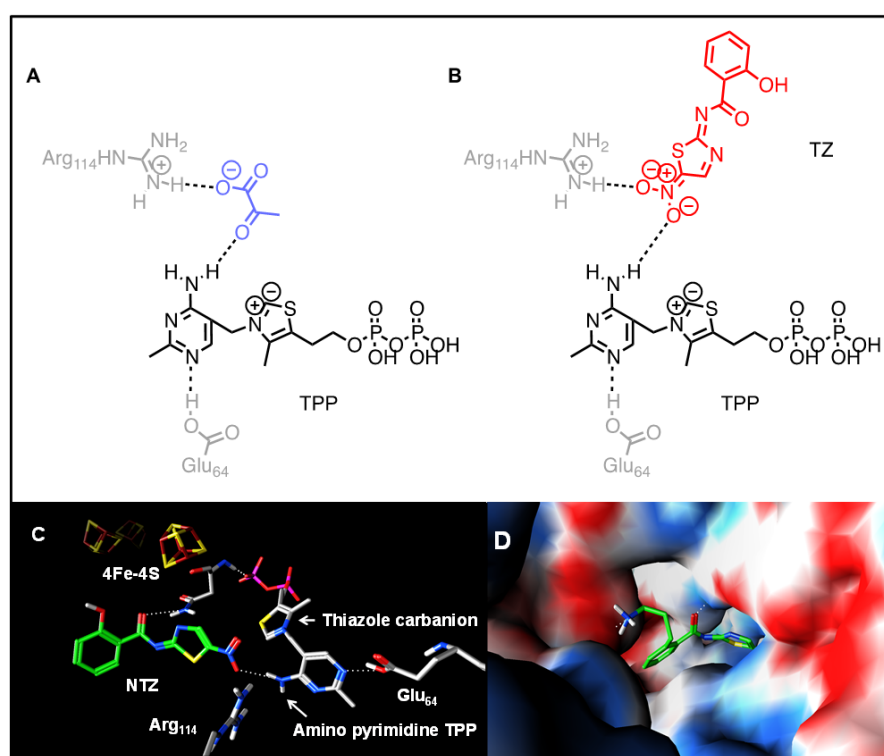


Figure 2. Docking simulations and mechanism of action. A. Interaction of pyruvate (blue) with the protonated N4' aminopyrimidine of TPP. B. Projected interaction of tizoxanide (TZ, red) with the N4' aminopyrimidine of TPP. C. Spatial orientation of nitazoxanide interacting with TPP based on docking simulation. D. Docking simulation showing amoxicillin in the pocket of PFOR.

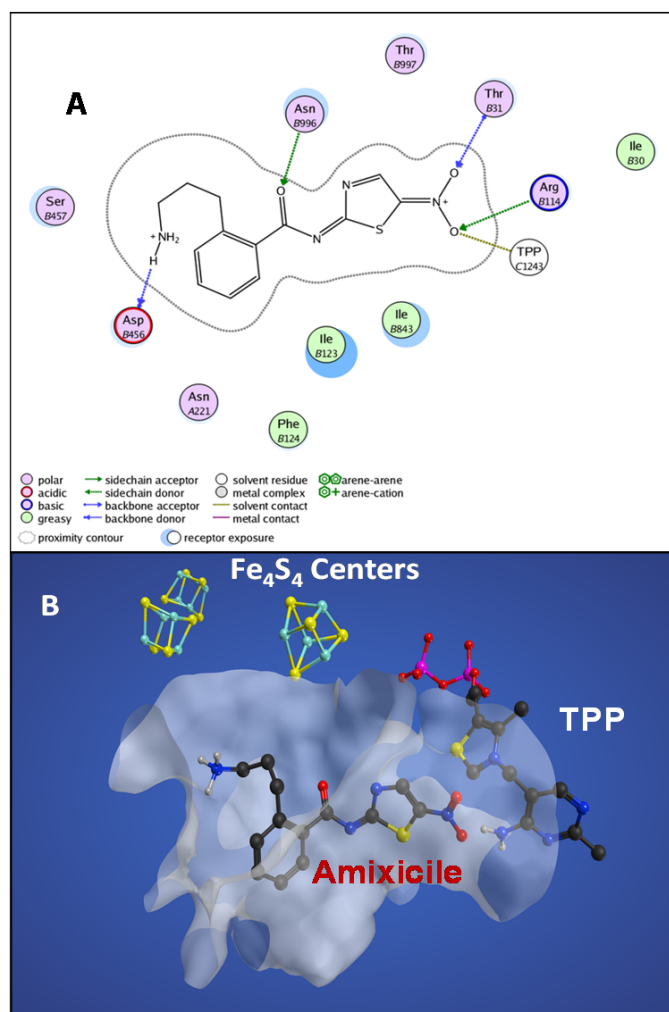


Figure 3. Amixicile presentation in the PFOR pocket. A. *In silico* docking studies suggest that the propylamine tail of amixicile forms an electrostatic interaction with aspartic acid residue. Note also the interactions with TPP and with Thr B31, Asn B996 and Arg B114. Image generated with MOE software. B. A crevice in the R² position of amixicile explains increased in vitro activity of substitutions at the R² position on the benzene ring.

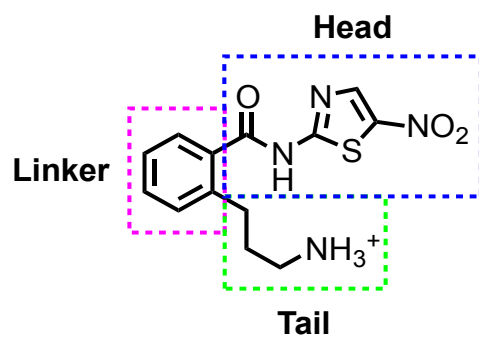


Figure 4. Inhibitor design from amoxicillin. The scaffold of amoxicillin was divided into three sections for second-generation SAR studies: the head group region (blue), linker region (pink) and tail region (green).

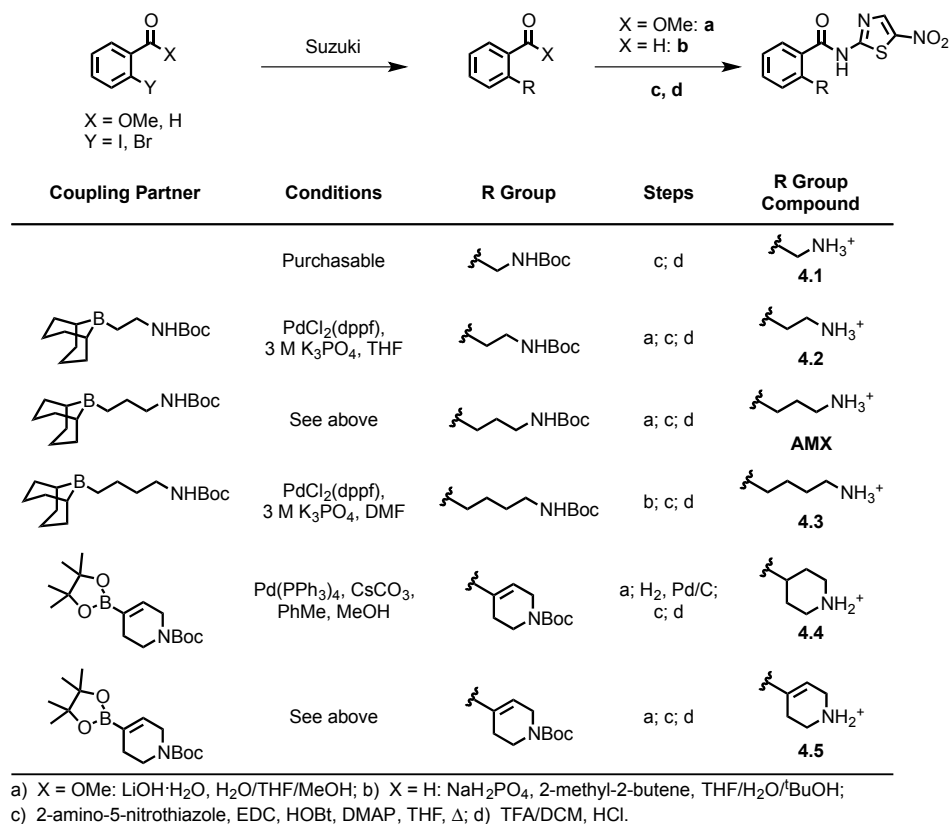


Figure 5. Chemical strategy for tail assemblies. Suzuki coupling was performed to append the desired amine tail to the methyl benzoate or benzaldehyde linker region, after which a Pinnick oxidation or saponification was performed to convert the carbonyl to the carboxylic acid. An EDC amide coupling was performed to attach the 2ANT head group followed by deprotection of the amino group.

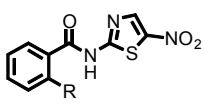
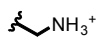
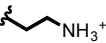
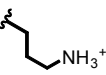
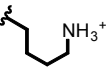
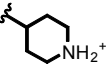
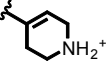
					
Compound	R Group	cLogP	PFOR Inhibition [40 μM], % ^a	MIC (μg/ml) <i>H. pylori</i> <i>C. difficile</i>	
4.1		0.46	51	4	n.d.
4.2		0.79	n.d.	n.d.	>10
AMX		1.17	75	0.5	0.125
4.3		1.70	91	2	1
4.4		1.81	88	8	4
4.5		2.81	95	4	1

Figure 6. Biological activity of R group tail constructs. The cLogP was inferred using ChemDraw. PFOR inhibition in triplicate was determined as the percent inhibition by compounds at 40 μM and indexed to NTZ which is 50% inhibition. MIC tests for *H. pylori* and *C. difficile* (μg/ml) and the results of triplicate determinations. N.d. means not determined.

R ¹ = F; 4.6	R ³ = CH ₃ 4.12
R ² = CH ₃ 4.7	R ³ = OCH ₃ 4.13
R ² = F 4.8	R ³ = CN 4.14
R ^{2,3} = F 4.9	R ³ = CF ₃ 4.15
R ² = Cl 4.10	R ³ = Cl 4.16
R ² = CF ₃ 4.11	R ³ = F 4.17

Analogue ^a	cLogP	PFOR Inhibition [Drug] = 40 μM (%)	MIC (μg/mL)		
			<i>H. pylori</i>	<i>C. difficile</i>	<i>C. jejuni</i>
NTZ	2.2	50	1	0.125	1
AMX	1.17	75	1	0.25	4
4.6	0.91	95	0.5	0.25	8
4.7	1.67	n.d.	1.5.	0.06.	n.d.
4.8	1.32	93	0.125	0.125	4
4.9	1.40	90	0.5-1	0.125	4
4.10	1.89	97	1	0.0625	4
4.11	2.08	93	0.5-1	0.0625	4
4.12	1.67	n.d.	1	0.06	4.
4.13	1.25	n.d.	0.5	0.125	8
4.14	0.67	n.d.	4	n.d.	4.
4.15	2.08	n.d.	1	0.125	8
4.16	1.89	94	0.5	0.164	4
4.17	1.32	86	1	0.125	8

Figure 7. Ring substitutions of the amoxicillin scaffold. The cLogP was determined with

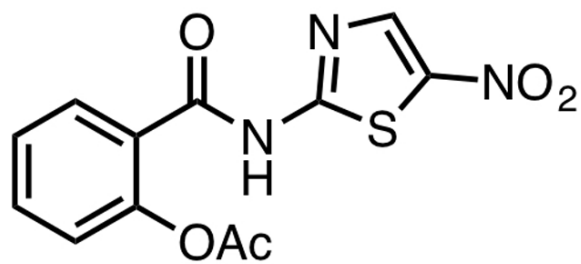
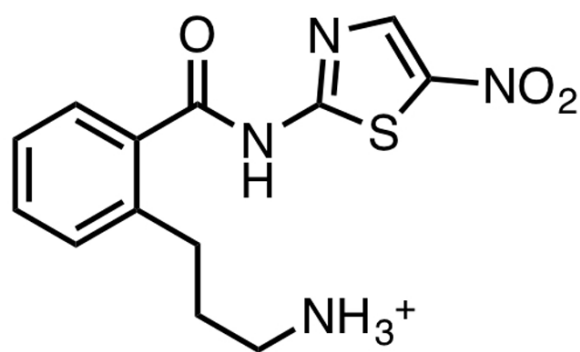
ChemDraw, PFOR inhibitory activity as described in Figure 6 and MIC determinations (μg/ml)

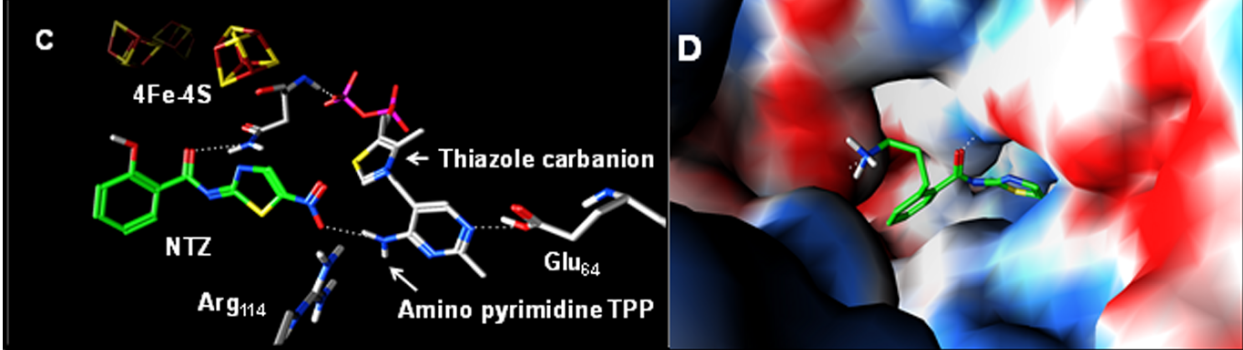
for *H. pylori*, *C. difficile* and *C. jejuni*. CC₅₀ determinations with HeLa cells (Alomar blue) were

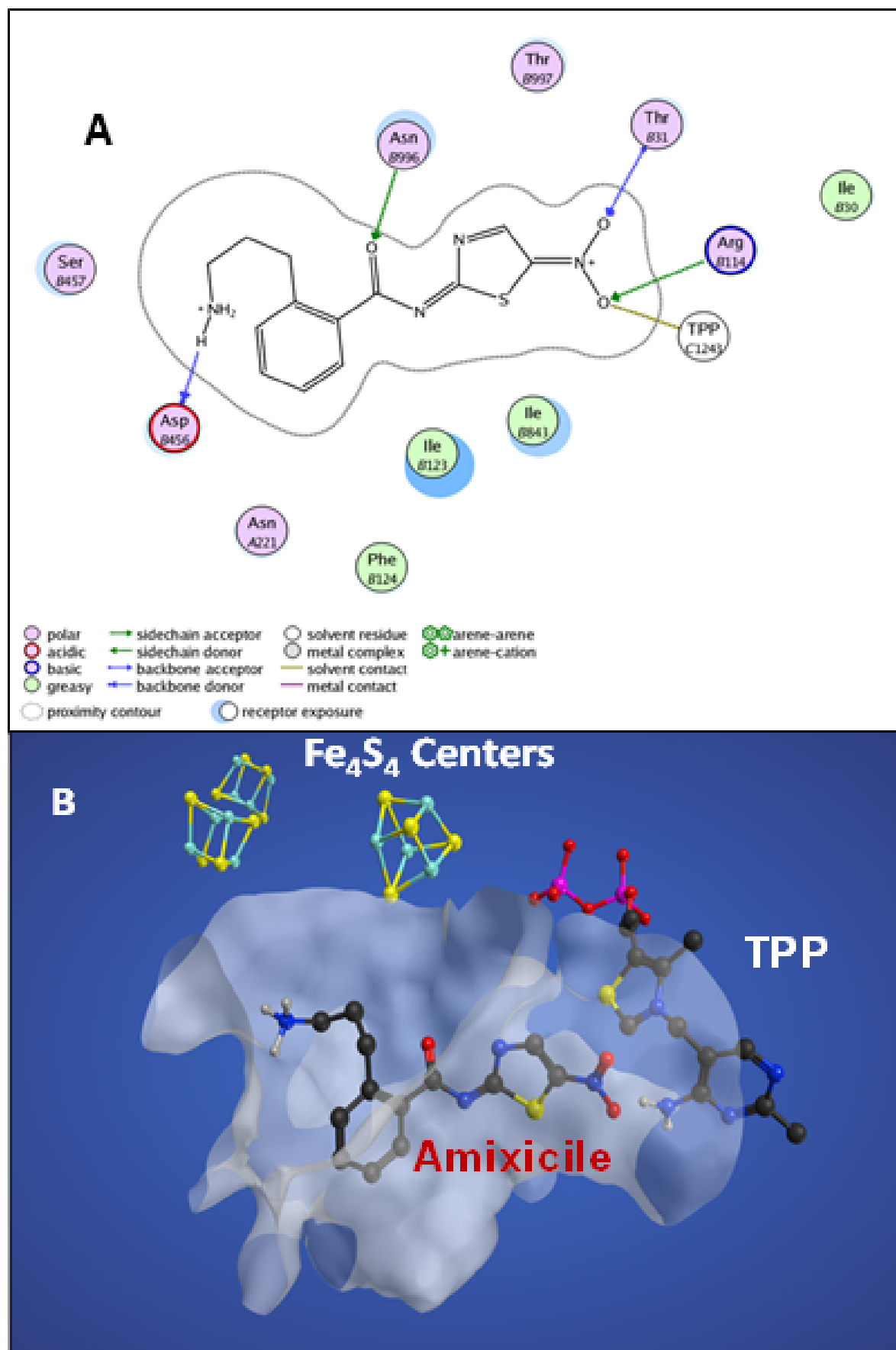
>100 μM and are not depicted. Not determined (n.d.). All MIC tests are the mean of 3 to 6

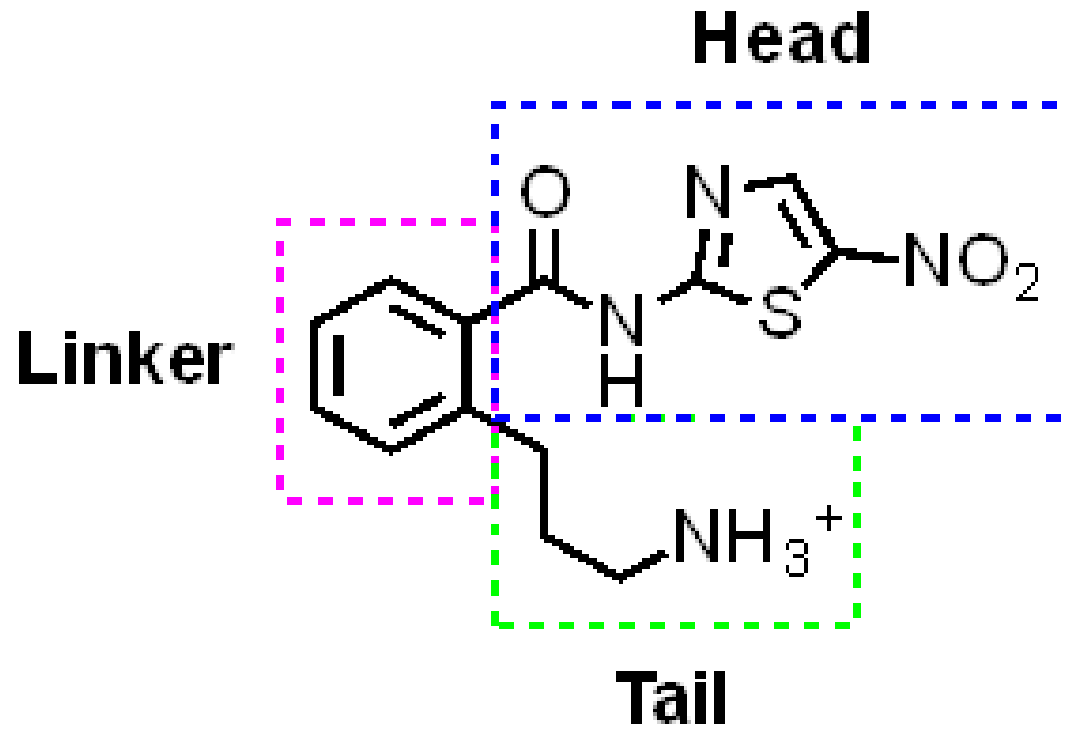
experiments performed in triplicate and for some analogues a range is presented.

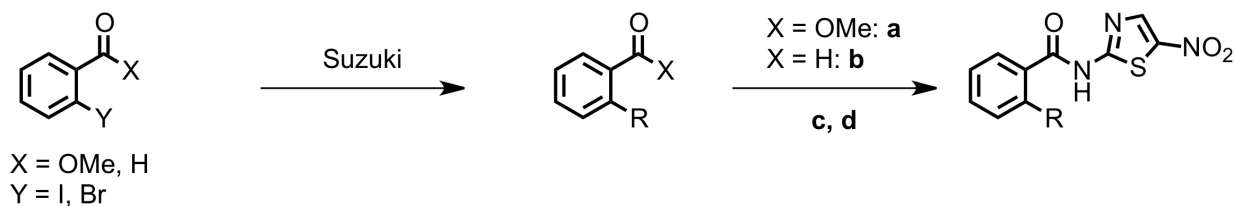
^aR = H unless otherwise noted.

**Nitazoxanide (NTZ)****Amixicile**



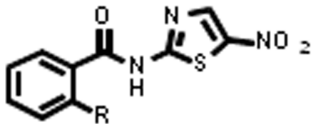


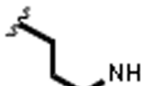
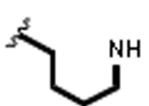
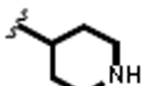
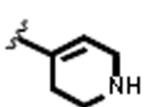


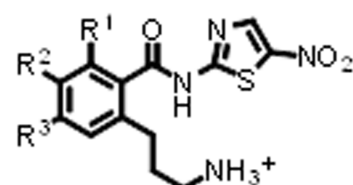




Coupling Partner	Conditions	R Group	Steps	R Group Compound
	Purchasable		c; d	 4.1
	$\text{PdCl}_2(\text{dppf})$, 3 M K_3PO_4 , THF		a; c; d	 4.2
	See above		a; c; d	 AMX
	$\text{PdCl}_2(\text{dppf})$, 3 M K_3PO_4 , DMF		b; c; d	 4.3
	$\text{Pd}(\text{PPh}_3)_4$, CsCO_3 , PhMe, MeOH		a; H_2 , Pd/C; c; d	 4.4
	See above		a; c; d	 4.5

a) $\text{X} = \text{OMe}$: $\text{LiOH} \cdot \text{H}_2\text{O}$, $\text{H}_2\text{O}/\text{THF}/\text{MeOH}$; b) $\text{X} = \text{H}$: NaH_2PO_4 , 2-methyl-2-butene, $\text{THF}/\text{H}_2\text{O}/t\text{BuOH}$;
 c) 2-amino-5-nitrothiazole, EDC, HOBT, DMAP, THF, Δ ; d) TFA/DCM, HCl.

					
Compound	R Group	cLogP	PFOR Inhibition [40 μ M], % ^a	MIC (μ g/ml) <i>H. pylori</i> <i>C. difficile</i>	
4.1		0.46	51	4	n.d.
4.2		0.79	n.d.	n.d.	>10
AMX		1.17	75	0.5	0.125
4.3		1.70	91	2	1
4.4		1.81	88	8	4
4.5		2.81	95	4	1


 $R^1 = \text{F}$ **4.6**
 $R^2 = \text{CH}_3$ **4.7**
 $R^2 = \text{F}$ **4.8**
 $R^{2,3} = \text{F}$ **4.9**
 $R^2 = \text{Cl}$ **4.10**
 $R^2 = \text{CF}_3$ **4.11**
 $R^3 = \text{CH}_3$ **4.12**
 $R^3 = \text{OCH}_3$ **4.13**
 $R^3 = \text{CN}$ **4.14**
 $R^3 = \text{CF}_3$ **4.15**
 $R^3 = \text{Cl}$ **4.16**
 $R^3 = \text{F}$ **4.17**
MIC ($\mu\text{g/mL}$)

Analogue ^a	cLogP	PFOR Inhibition [Drug] = 40 μM (%)	<i>H. pylori</i>	<i>C. difficile</i>	<i>C. jejuni</i>
HTZ	2.2	50	1	0.125	1
AMX	1.17	75	1	0.25	4
4.6	0.91	95	0.5	0.25	8
4.7	1.67	n.d.	1.5.	0.06.	n.d.
4.8	1.32	93	0.125	0.125	4
4.9	1.40	90	0.5-1	0.125	4
4.10	1.89	97	1	0.0625	4
4.11	2.08	93	0.5-1	0.0625	4
4.12	1.67	n.d.	1	0.06	4.
4.13	1.25	n.d.	0.5	0.125	8
4.14	0.67	n.d.	4	n.d.	4.
4.15	2.08	n.d.	1	0.125	8
4.16	1.89	94	0.5	0.164	4
4.17	1.32	86	1	0.125	8